Mayrhofer, Markus; Koller, Michael; Seemann, Peter; Bordbar, Hadi; Prieler, Rene; Hochenauer, Christoph

MILD combustion of hydrogen and air – An efficient modelling approach in CFD validated by experimental data

Published in:
International Journal of Hydrogen Energy

DOI:
10.1016/j.ijhydene.2021.11.236

Published: 29/01/2022

Document Version
Peer-reviewed accepted author manuscript, also known as Final accepted manuscript or Post-print

MILD combustion of hydrogen and air – An efficient modelling approach in CFD validated by experimental data

Markus Mayrhofer[a,*], Michael Koller[a], Peter Seemann[a], Hadi Bordbar[b], Rene Prieler[c], Christoph Hochenauer[c]

[a] Ebner Industrieofenbau GmbH, Ebner-Platz 1, 4060 Leonding, Austria
[b] Aalto University, Department of Civil Engineering, Rakentajanaukio 4A, Espoo, Finland
[c] Graz University of Technology, Institute of Thermal Engineering, Inffeldgasse 25/b, 8010 Graz, Austria
***Corresponding author. E-mail address: mhm@ebner.cc (M. Mayrhofer)**

Abstract

The present work deals with the development of an efficient modelling approach for the flameless combustion of pure hydrogen with highly preheated air. It contains an application of different flamelet-based combustion models to achieve convergence in a computationally cheap way in contrast to time consuming methods such as the Eddy Dissipation Concept (EDC) model. Moreover, an evaluation of three detailed reaction mechanisms for the application of flameless hydrogen combustion is also included. The selection and implementation of a “Weighted Sum of Grey Gas” (WSGG) model to predict the radiative heat transfer as accurate as possible constitutes another important goal in the present work. The results of all modelling approaches were compared with extensive temperature measurements in the reaction zone. Additional temperatures of the test rig’s control thermocouples were also compared with the results of the simulation to strengthen the validation. Maximum temperature deviation in the burner’s axis of about 50 K can be achieved. Furthermore, the experimental and numerical results in this paper were compared with the results of flameless combustion of natural gas at equal furnace conditions and the same burner test rig. Higher temperatures in the burner axis up to a distance of 1855 mm were observed at hydrogen operation with a maximum difference of about 150 K to the natural gas case. A concluding evaluation of the furnace efficiency showed an

increase by about 7 percent by changing the fuel from natural gas to hydrogen. This is achieved by reduced flue gas loss and an improved heat transfer.

1. Introduction

With the invention of flameless oxidation (FLOX) [1], also known as “Moderate or Intense Low-oxygen Dilution” (MILD) combustion [2, 3] a promising technology for reducing thermal nitrogen oxide (NOx) formation was found. Remaining within present and future national emission limits, especially in industrial furnaces [4, 5], is achievable without any additional secondary waste gas treatment systems which lead to a reduction in process efficiency [1]. Because international climate agreements have been signed [6, 7], not only the nitrogen oxide emissions but also carbon dioxide emissions must be reduced to the lowest possible level. In the European Union, a tax for carbon dioxide emissions has been introduced [7]. Emitters must own certificates which limit the maximum emissions and they are obliged to pay for each ton of emitted CO_2 [8]. Driven by this, the combustion of fuels, which produces less carbon dioxide than natural gas, is gaining more interest. An upcoming approach to reduce CO_2 emissions of combustion systems is the addition of hydrogen to the original fuels or their complete replacement, which is natural gas in many cases. Especially green hydrogen [9], which is produced using renewable sources [10, 11], could be a sustainable option as fuel for combustion processes. This approach was evaluated for the application in heat treatment furnaces in a previous study [12] and showed a potential in decreasing carbon dioxide emissions and increasing furnace efficiency.

1.1. Hydrogen combustion application

A great number of experimental and numerical studies have been performed in the flameless combustion technology [1, 13] since its invention in the early 1990’s. As a result, the process is well explored for natural gas with the benefits of a very stable combustion and homogeneous temperature distribution in the reaction zone [2]. Additionally, research has been done on the flameless combustion technology for liquid [14, 15] and solid fuels [16, 17] as well. Derudi et

al. [18] present an experimental study which shows that the application of MILD combustion with “Coke Oven Gas” (COG) is also possible. This fuel gas has a typical hydrogen content of about 60 vol.% which leads to higher nitrogen oxide emissions in comparison to natural gas. Considering this investigation, one can expect that flameless combustion of pure hydrogen is also possible. It has also been found that nitrogen oxide emissions increase when hydrogen is added to the fuel supply of natural gas burners operating in flame [19] and flameless combustion [12]. This resulting effects on the combustion process and the formation of additional nitrogen oxides have to be considered for design and operation of new hydrogen burners. Fundamental experimental work in flameless combustion of natural gas / hydrogen blends using chemiluminescence was performed by Ayoub et al. [20] in a laboratory furnace. Several fuel gas blends from pure natural gas to pure hydrogen were applied. The authors showed that very low NOx emissions are achievable by combusting pure hydrogen under MILD conditions without air-preheating but with the drawback of reduced combustion efficiency. An investigation of the flow field in a co-flow burner using “Particle Image Velocimetry” (PIV) shows increased turbulent intensity by adding 25 vol. % hydrogen to natural gas [21]. Further experimental work with different hydrogen mixtures to natural gas in lab-scale furnaces can be found in the bibliography [22, 23].

1.2. CFD modelling methodologies for hydrogen combustion

The addition of hydrogen to natural gas leads to complex effects when applying MILD or flameless combustion, which must be modelled in “Computational Fluid Dynamics” (CFD) simulations [24]. To capture this behaviour in the reaction zone, an application of detailed reaction mechanisms is necessary, which was found by several researchers [24, 25]. Ivarone et al. [26] modelled the JHC Co-flow burner under MILD conditions with different hydrogen contents up to 9 vol.% in the natural gas. The authors used the Eddy Dissipation Concept (EDC) model with the KEE-58 [27] mechanism to include the prediction of nitrogen oxide

formation in their simulation. An investigation of a flameless radiant tube burner with hydrogen enriched natural gas up to 20 vol. % was performed by Parente et al. [25]. The combustion model and reaction mechanism evaluation show that the EDC model with the detailed mechanisms GRI 3.0 [28] and KEE-58 [27] predicts promising results according to the experimental data. Galletti et al. [24] investigated a lab-scale burner fed with a highly hydrogen enriched fuel (60 vol.%) and operated it in MILD and flame combustion. Eddy Dissipation / Finite Rate (EDM/FR) with a two-step mechanism and the EDC with the detailed schemes KEE-58 [27], DRM-19 [29] and GRI 3.0 [28] were applied. The best accordance with the experimental data was achieved with GRI 3.0 [28]. Cellek and Pinarbasi [30] investigated a low swirl burner with different methane / hydrogen blends using CFD. The hydrogen content in the blends rises from 25 to 75 vol.%. The authors used the EDM model in combination with a modified two step reaction mechanism and observed increased temperature peaks and NOx emissions at higher hydrogen contents. Flameless combustion with different natural gas / hydrogen mixtures from pure natural gas to pure hydrogen were investigated by Cellek [31]. In this study, the chemical reactive flow was captured with the EDC model and the detailed mechanism GRI 2.11 [28]. Furthermore, the paper presents the influence of the turbulence model on the predicted results. Different hydrogen enrichments of methane and syngas were investigated with the EDC model for their application in MILD combustion in the work of Mardani et al. [32]. It was found that hydrogen enrichment of syngas leads to a better combustion situation in comparison to the methane hydrogen mixtures. A modified EDC model approach was presented by Mardani [33], which was validated with experimental data. This paper proposes guidelines for adjusting the semi empirical model constants to achieve an improved prediction for MILD combustion. Further investigations in well-suited constants for the EDC are proposed by De et al. [34]. Instead of using global model constants, Parente et al. [35] suggested an approach for a local prediction of EDC coefficients depending on the Reynolds and Damköhler number. Another work of Aminian et al. [36] improved the local extinction prediction of the EDC for

MILD combustion. The prediction of nitrogen oxide (NOx) formation in MILD combustion with hydrogen enriched natural gas or pure hydrogen is another crucial task for modelling [37]. In addition to the well-known thermal [38] and the prompt [39] formation route, the NNH route by Konnov [40] and the N2O route [41] must be considered by the application of natural gas / hydrogen fuels [42, 43]. Studies in the field of predicting the NOx emissions of hydrogen enriched natural gas in CFD used reduced kinetic schemes, which include these four formation routes [44, 45, 37, 46]. The consideration of the radiative heat transfer is an important issue in combustion modelling which was solved using the “Discrete Ordinate” (DO) model [47, 48] in several papers [24, 25]. The absorption coefficient is determined by the “Weighted Sum of Grey Gas” (WSGG) model with the coefficients from Smith et al. [49] for hydrogen enriched natural gas up to a content of 20 vol.%. Higher hydrogen enrichments of up to 100% in the fuel, change the flue gas composition and therefore, the applicability of the commonly used WSSG model must be proven. An evaluation of modelling approaches for pure hydrogen combustion [50] presented further WSGG model parameters based on correlations concerning gas emissivity in the literature. It was found that the investigated WSGG model including other coefficients [51] predicts better results in comparison to Smith et al. [49]. Furthermore, extended WSGG models were presented by Yin et al. [52] and Bordbar et al. [53, 54] which captured a wide range of steam and carbon dioxide mixtures.

1.3. Objective

It becomes evident that numerous studies investigating the MILD combustion of natural gas / hydrogen blends are presented in the literature with valuable results, especially in CFD modelling [25, 24, 31, 55, 56, 57, 58]. Most of them use the EDC model in conjunction with a detailed reaction mechanism with the drawback of computationally expensive calculations. However, to the best of the authors’ knowledge, there had not been any studies which evaluated flamelet-based combustion models and WSGG models on the MILD combustion of pure

hydrogen with pre-heated air including a validation with experimental data. Thus, the following points are investigated in this paper:

- Experimental temperature field measurement in the reaction zone at flameless combustion with pure hydrogen and preheated air.

- Evaluation of flamelet-based combustion models, detailed reaction mechanisms and WSGGM approaches for their application to predict a flameless hydrogen burner with preheated air.

- Development of an efficient model approach to perform parameter studies in the field of flameless burner development and their integration in furnaces.

- Comparison of the heat transfer and furnace efficiency by using flameless combustion under natural gas and pure hydrogen with air as oxidizer.

2. Furnace description – Burner test rig

The observed burner test furnace in this work is designed for the investigation, development and optimization of industrial gas burners under different operating conditions. A schematic overview with the main components is presented in Figure 1. The test rig consists of an outer steel construction with a 375 mm thick ceramic fibre insulation on the inside. Hot flue gases leave the combustion chamber in a vertical chimney, where the main gas composition and emissions can be determined. A regulation of the temperature inside the furnace is made possible by 6 ceramic radiant tubes. Three of them are located at the combustion chamber's top, which only have a cooling function. The other ones are located at the bottom and can operate as radiant heating tubes and as cooling tube as well. The temperature observation is done by control thermocouples, which are located at the top of the furnace (TC1, TC2, TC3) and a flameless supervision thermocouple on a side wall

(TC_FL). The test burner is located on the front side in the central longitudinal axis to ensure no influence of the inner geometry on the reaction zone. Discrete measurement positions along the burner's axis allow temperature and species concentration measurements with an aspirating pyrometer. The operation temperature in this work is set to about 1150°C in each furnace thermocouple (TC1, TC2, TC3), which is a representative value for continuous stainless-steel annealing furnaces. Preheated combustion air with a temperature of 450°C is provided by an external electrical air-preheater. The heat flux on the ceramic tubes can be measured and used as boundary conditions for the CFD simulation. Several measurements were performed with a residual oxygen content of 3 vol.% in the dry flue gas. The investigated burner is an ECOBURN FL burner, which can operate under air-staged and flameless mode. Different operating conditions can be achieved according to their application in heat treatment furnaces for steel, aluminium and copper-based alloys, which are the main application areas. Only the flameless case using pure hydrogen as fuel gas is observed in this work at a thermal fuel input of 155 kW. Later, a comparison with the flameless combustion of natural gas at the same furnace system will be done (see [59]). A more detailed description of the investigated burner, the test rig and a correction method for the measured temperature field is presented in a previous work [59].

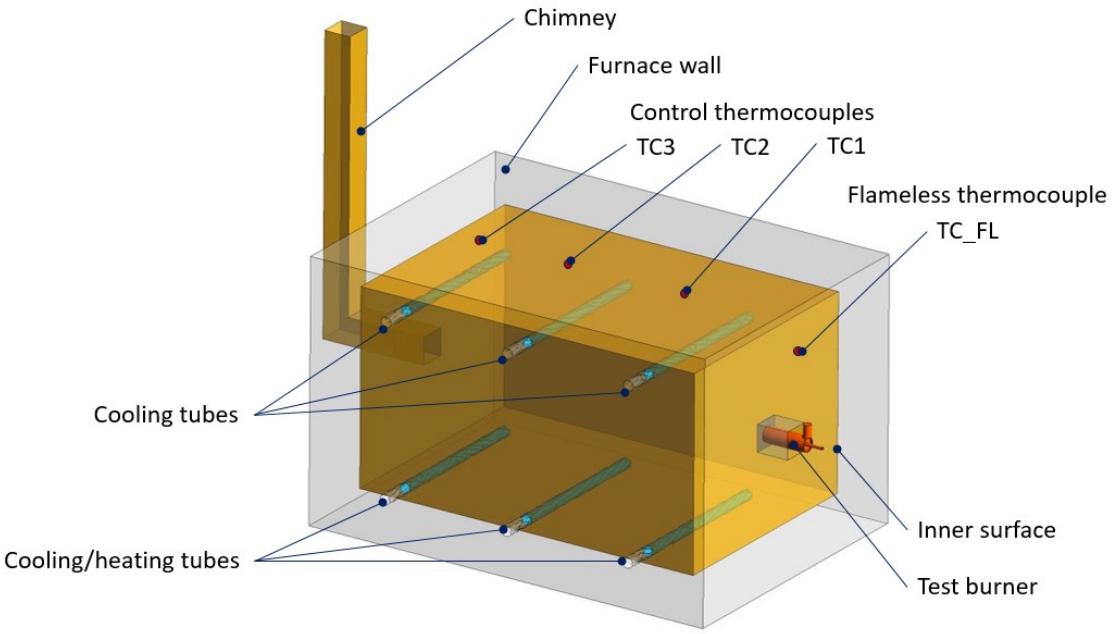

Figure 1.: Schematic model of the burner test rig and measurement positions

3. Numerical Setup

3.1. Turbulent flow modelling

The turbulent flow inside the burner test rig was calculated using the Favre-averaged Navier-Stokes equations (Eq. 1 & 2). All numerical simulations in this paper are steady-state and were performed with the commercial code ANSYS Fluent 2020 R1. Incompressible gas behaviour was assumed because of the low Mach numbers and the density fluctuations caused by temperature gradients were considered using the ideal gas law. For the solution procedure, a double precision, pressure-based coupled solver was chosen. The continuity and momentum equations were solved with the coupled algorithm for the pressure-velocity coupling and the pressure staggering option (PRESTO!) [60] was used for pressure discretisation. All other transport equations were discretised by a Monotonic-Upstream centred Scheme for Conversation Laws (MUSCLE). Only the radiative heat transfer was spatially discretized with the first-order upwind scheme, because of a low optical thickness of 0.36 [61]. Higher discretization schemes for radiative heat

transfer are suggested for higher optical thicknesses [61]. Gradients were calculated with the Least-Square method.

$$\frac{\partial}{\partial x_i}(\bar{\rho}\tilde{u}_i) = 0 \tag{1}$$

$$\frac{\partial}{\partial x_j}\left[\bar{\rho}\tilde{u}_i\tilde{u}_j + \bar{p}\delta_{ij} + \overline{\rho u_i'' u_j''} - \overline{\tau_{ij}}\right] = 0 \tag{2}$$

The Reynolds stresses ($\overline{\rho u_i'' u_j''}$) in Eq.2 were modelled with the realizable k-ε model proposed by Shih et al. [62]. This turbulence closure is a modification of the standard-k-ε-model and is suitable for predicting flows with strong streamline curvatures and the spreading rates of axisymmetric jets [61]. Two equation turbulence models are widely used in industrial applications and different jet burner investigations [63, 64, 65] showed positive results with this approach. The standard wall function was applied for the near wall treatment because of typical y^+ values of about 25 [61]. Constant monitors of the control thermocouples and flue gas temperatures with a maximum fluctuation of 5 K were used to identify the convergence of the solution. Furthermore, all residuals were below 10E-03 and the overall mass and heat imbalance was lower than 0.1%.

3.2. Combustion modelling

In combustion modelling, chemical kinetics and turbulent mixtures are, depending on the case, problematic. The task for combustion modelling in this study is given by the flameless combustion of pure hydrogen as fuel and highly pre-heated air as oxidizer. A suitable selection of the turbulence/chemistry interaction model and the reaction mechanism affects the computing time in general. Some researchers [24] used the EDM/FR model which is a modification of the original EDM proposed by Magnussen and Hjertager [66]. This model calculates, in addition to the Eddy Dissipation Rate, the Arrhenius Rate as well. The smaller one is then used for the calculation. A drawback of this approach is the limitation to two chemical reactions. To use detailed mechanisms

including radicals such as OH, many researchers use the EDC model from Magnussen [67] which is an improvement of the EDM. This model assumes that the reaction takes place in fine scales. The disadvantage of this approach is the long calculation time for chemistry integration. To capture the task in this paper with low computational costs, although detailed reaction mechanisms should be used, the steady flamelet combustion model (SFM) is applied. Different variants of the SFM were successfully applied and validated for flameless combustion with the used "ECOBURN FL" burner in previous studies [59, 68]. In this approach, the turbulent flame is described as an ensemble of small, laminar one-dimensional flamelets [69, 70]. These flamelets are usually represented by counter-flow diffusion flames. In such flamelets, density, species mass fractions and temperatures can be calculated by detailed mechanisms and compared with measurements. The flamelet, or the thermochemical state in the flamelet, is defined by the mixture fraction f (Eq.3) and the scalar dissipation $\chi = 2D|\nabla f|$ (similar to the strain rate). Computational extensive chemistry calculations of the flamelet were pre-processed and stored in look-up tables. The advantage of this model is the calculation of a turbulent reactive flow with a detailed chemical reaction mechanism by solving only two additional transport equations for the Favre-averaged values $(\tilde{f}, \widetilde{f''^2})$ (Eq.6 and 7), with $f' = f - \tilde{f}$. A disadvantage of the SFM model is the assumption of a fast chemistry, where effects far away from equilibrium, like local extinction, flame lift off and ignition delay cannot be predicted [61]. Small deviations from the equilibrium are however considered by the scalar dissipation ($\chi > 0$).

$$f = \frac{Z_i - Z_{i,ox}}{Z_{i,fuel} - Z_{i,ox}} \tag{3}$$

$$\nabla\left(\bar{\rho}\vec{u}\tilde{f}\right) = \nabla\left(\frac{\mu_t}{\sigma_t}\nabla\tilde{f}\right) \tag{4}$$

$$\nabla\left(\bar{\rho}\vec{u}\widetilde{f''^2}\right) = \nabla\left(\frac{\mu_t}{\sigma_t}\nabla\widetilde{f''^2}\right) + C_g\mu_t\left(\nabla\tilde{f}\right)^2 - C_d\bar{\rho}\frac{\epsilon}{k}\widetilde{f''^2} \tag{5}$$

In addition to the "Non-Premixed Steady Flamelet Model" (NP-SFM), the Partially Premixed Flamelet Generated Manifold (PP-FGM) model

proposed by van Ojien and de Goey [71] was applied. This model parameterizes the flamelet over the mixture fraction and reaction progress variable c (Eq.8) instead of the strain rate. This has the benefit that ignition delay and full flame quenching can be achieved in the model [61]. As a result, two more transport equations must be solved for reaction progress and reaction progress variance. Furthermore, an extended flamelet model was evaluated (PP-SFM). This solves one additional equation for the reaction progress variable without variance. The three different detailed reaction mechanisms “GRI 3.0” [28], “San Diego Mechanism” [72] and the mechanism of O’Conair et al. [73] were evaluated for their application in modelling flameless hydrogen combustion.

$$c = \frac{Y_c}{Y_c{}^{eq}} = \frac{\sum_k a_k (Y_k - Y_k^u)}{\sum_k a_k (Y_k^{eq} - Y_k^u)} \tag{6}$$

3.3. Thermal radiation modelling

The “Discrete Ordinate” (DO) model [47, 48] was used to predict the radiative heat transfer between the furnace walls, flue gas and the ceramic tubes in the burner test rig. Within the methodology, an angular discretization into azimuth and polar angle is done for each octant. The “Radiative Transfer Equation” (RTE) (Eq. 7) is solved for each direction $\vec{s}$ and gray gas assumption. $I(\vec{x},\vec{s})$ denotes the radiation intensity depending on the position and the direction vector, k represents the absorption coefficient of the flue gas, σ_s is the scattering coefficient, n is the refractive index, $\vec{s}$ is the direction of scattered radiation, Φ is the phase function and Ω the solid angle. The optical thickness is modelled with the second term on the left-hand side of Eq. 7 and determines the loss of radiation intensity due to scattering and absorption in the gas phase. Since there are no particles in the gas phase, the refractive index and the scattering coefficient were set to values of 1 and $0\ m^{-1}$ .Each octant was discretized with 4x4 solid angels leading to an overall number of 128 directions for the radiative heat transfer.

$$\frac{dI(\vec{x},\vec{s})}{ds} + (k+\sigma_s)I(\vec{x},\vec{s}) = kn^2\frac{\sigma T^4}{\pi} + \frac{\sigma_s}{4\pi}\int_0^{4\pi} I(\vec{x},\vec{s}')\Phi(\vec{x},\vec{s}')\,d\Omega \quad (7)$$

$$k_{gray} = -\frac{1}{S}\ln(1-\varepsilon) \quad (8)$$

The calculation of the absorption coefficient with gray gas assumption (Eq.8) can be performed with different sets of coefficients for the WSGG model. The total emissivity ε may be represented by the sum of the emissivity of N hypothetical gray gases weighted by temperature-dependent factors and can be written according to Eq.9, where $a_{\varepsilon,i}$ is the temperature dependent weighting factor of the i-th gray gas band. For a gas mixture, k_i is the absorption coefficient and P is the sum of the partial pressures of the participating gases. The equivalent-length according to the domain-based approach [74] $S = 3.6\,V/A$ has a value of 1.36 m for the burner test rig.

$$\varepsilon = \sum_{i=0}^{N} a_{\varepsilon,i}(T)[1-e^{-k_i PS}] \quad (9)$$

Most of the existing WSGGMs are developed for hydrocarbon combustion, either for air-fuel or for oxy-fuel conditions [52, 75, 76, 49, 77]. One of them is the well-known model by Smith et al. [49] for air-fuel cases, which is mostly implemented in commercial CFD codes. Yin [78] refined this model for the application in oxy-fuel combustion [79]. The implementations and limitations of these approaches [49, 78] are presented in Table 1 and 2. In hydrogen-air cases, the flue gas mainly consists of steam, nitrogen and the residual oxygen. Since the importance/impact of H_2O vapor partial pressure (P_W) on radiation heat transfer is much larger than that of CO_2 (P_C), it would be beneficial to derive a new WSGGM for hydrogen combustion, without the CO2 involvement (P_C) in the existing models. Based on the existing WSGGMs, an alternative way for the simulation of MILD combustion of hydrogen would be the implementation of a part of the refined air-fuel WSGGM [78] in the following way: If $P_W \leq 0.01$, the table $P_W \to 0$ should be used, otherwise if $P_W \leq 0.2$, use the table $P_W = 0.05$ and for values of $P_W > 0.2$, the $P_W = 1$ table is applied. Moreover, the model by Bordbar et al. [54], which covers the full range of H_2O / CO_2 ratios was also evaluated in this work. The model is developed for a pressure of 1 atm and a pathlength

range from 0.01 to 60 m. Furthermore, the non-gray DO model offers a more comprehensive method to increase the accuracy of the predicted heat flux [80]. In this approach, the entire spectrum is divided into small intervals or fractions and one RTE per direction is solved for each interval or fraction. The radiative intensity I_i and absorption coefficient k_i will be used in the simplified RTE (Eq.10), where a_i denotes the percentage of the total blackbody radiation that belongs to the i-th spectral fraction.

$$\frac{dI_i}{ds} = k_{a,i}\left(a_i \frac{\sigma T^4}{\pi} - I_i\right) \tag{10}$$

Table 1: Details of the WSGGMs of Smith et al. and Yin: Derivation, Formulation, and Implementation of the Models [78]

	Smith et al. WSGGM	**refined/extended WSGGM**
reference model	EWBM	EWBM
	(1) Emissivity Database Generated Using the Reference Model: Summary of the Conditions	
total pressure, P_T (atm)	1 atm	1 atm
gas temperature, T_g (K)	600−2400 K, with an interval of 50 K	500−3000 K, with an interval of 25 K
PL ≡ (P_W + P_C)L (atm m)	0.001−10 atm m; 12 discrete values	beam length, L = 0.001−60 m; 146 values
representative conditions		
	(1) carbon dioxide: $P_C \rightarrow 0$ atm	(1) carbon dioxide: $P_C \rightarrow 0$ atm
	(2) gas mixture: P_W/P_C = 1 (Pc = 0.1 atm)	(2) gas mixture: P_W/P_C = 0.05 (P_C = 0.1 atm)
	(3) gas mixture: P_W/P_C = 2 (Pc = 0.1 atm)	(3) gas mixture: P_W/P_C = 1 (P_C = 0.1 atm)
	(4) water vapor: $P_W \rightarrow 0$ atm	(4) gas mixture: P_W/P_C = 2 (P_C = 0.1 atm)
	(5) water vapor: P_W = 1 atm	(5) water vapor: $P_W \rightarrow 0$ atm
		(6) water vapor: P_W = 0.05 atm
		(7) water vapor: P_W = 1 atm
	(2) WSGGM: With Coefficients Evaluated from Fitting to the Emissivity Database	
total emissivity, ε	eqs 9 where I = 3 and J = 4; model parameters (k_i and $b_{\varepsilon,i,j}$) seen in Smith et al.	eqs 9 where I = 4 and J = 4; model parameters (k_i and $b_{\varepsilon,i,j}$) summarized in Table 2
	(3) WSGGM Implementation: To Account for Variations in CO2 and H2O Vapor Concentrations in a Flame	
gray implementation	if ($P_W \leq 0.5$Pc), use Pc → 0 atm table else if ($P_W \leq 1.5P_C$), use (P_W/P_C) = 1 table else if ($P_W \leq 2.5P_C$), use (P_W/P_C) = 2 table else if ($P_W \leq 0.5$), use $P_W \rightarrow 0$ atm table else, use P_W = 1 atm table	if ($P_W \leq 0.01P_C$), use $P_C \rightarrow 0$ atm table else if ($P_W \leq 0.5P_C$), use (P_W/P_C) = 0.005 table else if ($P_W \leq 1.5P_C$), use (P_W/P_C) = 1 table else if ($P_W \leq 2.5P_C$), use (P_W/P_C) = 2 table else if ($P_W \leq 0.01$), use $P_W \rightarrow 0$ atm table else if ($P_W \leq 0.2$), use P_W = 0.05 atm table else, use P_W = 1 atm table

In non-gray gas modelling with WSGG models, the RTE should be solved for each of the gray gases of the WSGG models. The total (spectrally integrated) intensity is then calculated by the sum of the individual intensities. Hence, the computational cost of the non-gray modelling is higher than that of gray models. Nonetheless, the CPU increment is not essentially proportional to the number of the required extra RTE solutions in non-gray models as it depends on the share of radiation calculation in overall computational cost of the CFD calculations. However, with non-gray modelling there is no need for estimation of path length and the results are superior.

Table 2: Coefficients for the Refined and Extended WSGGM for Air-Fuel Flames [78]

band i	k_i	$b_{\varepsilon,i,1}$	$b_{\varepsilon,i,2}$	$b_{\varepsilon,i,3}$	$b_{\varepsilon,i,4}$
Carbon Dioxide, $P_C \rightarrow 0$ atm					
1	0.163233	0.204623	−0.378060	0.666639	−0.203453
2	13.096584	−0.020227	0.256006	−0.195201	0.040493
3	175.474735	0.044221	0.003850	−0.020175	0.004919
4	1310.847307	0.039311	−0.054832	0.025370	−0.003891
Mixture, P_W/P_C = 0.05 (Pc = 0.1 atm)					
1	0.352505	0.315106	0.023475	−0.057930	0.008408
2	8.210621	0.092474	0.109146	−0.121000	0.027145
3	137.410012	0.031702	0.037396	−0.040731	0.008742
4	1269.710976	0.046138	−0.061392	0.027164	−0.003996
Mixture, P_W/P_C = 1 (Pc = 0.1 atm)					
1	0.261021	0.500119	−0.447068	0.286878	−0.059165
2	3.147817	0.071592	0.508252	−0.384253	0.073477
3	54.265868	0.155320	−0.104294	0.014096	0.001643
4	482.900353	0.072615	−0.100601	0.046681	−0.007224
Mixture, P_W/P_C = 2 (Pc = 0.1 atm)					
1	0.179160	0.542458	−0.658411	0.466444	−0.100186
2	2.388971	0.101734	0.518429	−0.386151	0.073453
3	28.415805	0.146066	−0.008745	−0.058325	0.015984
4	253.059089	0.129511	−0.187993	0.090709	−0.014493
Water Vapor, $P_W \rightarrow 0$ atm					
1	0.085523	0.966357	−0.790165	−0.050144	0.115202
2	0.475777	0.662059	−2.262877	2.309473	−0.572895
3	8.549733	0.060870	0.436788	−0.395493	0.085146
4	201.906503	0.103568	−0.153135	0.074910	−0.012091
Water Vapor, P_W = 0.05 atm					
1	0.232724	0.340618	−0.105469	0.068051	−0.017828
2	2.134299	0.175818	−0.063466	0.086631	−0.026581
3	9.266065	0.044325	0.288376	−0.258205	0.054333
4	134.988332	0.126628	−0.186480	0.090755	−0.014569
Water Vapor, P_W = 1 atm					

1	0.065411	−0.077336	0.661776	−0.362515	0.053534
2	0.696552	0.506777	−0.758948	0.516146	−0.102909
3	4.862610	−0.079989	0.851078	−0.604264	0.113500
4	60.255980	0.373898	−0.540887	0.258923	−0.040957

aP_T = 1 atm; 0.001 ≤ L ≤ 60 m; 0.001 ≤ PL ≡ (P_W + P_C)L ≤ 60 atm m; and 500 ≤ T_g ≤ 3000 K.

3.4. Mesh and Boundary conditions – Burner test rig

The investigated burner test furnace was evaluated in a previous work [59], which includes a grid independency study and an evaluation of different spatial discretisation methodologies of the computational domain. It was found that a hybrid polyhedral / hexahedral mesh predicts the best results according to the experimental data. Thus, the mesh adjustments were reused in this study but nevertheless, meshes with refined reaction zones were investigated to ensure the grid independency. The applied meshes have about 1,334,000 (Mesh 1), 2,254,000 (Mesh 2) and 2,855,000 (Mesh 3) cells. A detailed wall resolution with inflation was not realized because the influence of near wall modelling on the velocity and temperature in the burner region is negligible. This has also been verified for high temperature furnaces in the literature [63]. The mesh quality can be specified with a maximal aspect ratio of 12 and an orthogonal skewness of 0.84. Details of the used hybrid polyhedral / hexahedral meshes are shown in Figure 3. The reaction zone was discretised with very fine hexahedral cells. It can be observed that the major part of the furnace was also made with hexahedrons. The transition from the reaction zone and the ceramic tubes to the global combustion chamber domain was made with polyhedrons. The investigated burner is operated with a thermal input of 155 kW and preheated combustion air. The hydraulic diameter and the turbulent intensity with a value of 5% were set as turbulence boundary conditions at the inlets. All boundary and operation conditions for steady state operation of the furnace at 1150°C are summarized in Table 3.

Table 3: Boundary and operation conditions

Coupled wall boundary condition on inner surface wall		
Internal emissivity	[-]	0.75
Convective boundary condition at outer wall		
Free stream temperature	[°C]	20
Heat transfer coefficient	[W/m²K]	30
Internal emissivity	[-]	0.9
Material properties of the furnace walls		
Density	[kg/m³]	170
Thermal conductivity	[W/mK]	0.38
Specific heat capacity	[J/kgK]	800
Heat Flux boundary conditions on the ceramic tube walls		
Internal emissivity	[-]	0.965
Heat flux cooling tubes	[W/m²]	-21599
Heat flux heating tubes	[W/m²]	-10806
Mass-flow inlet for the fuel (100 vol.% H2)		
Mass-flow rate	[kg/s]	0.001235
Temperature	[°C]	25
Mass-flow inlet for the oxidizer (79 vol.% N2, 21 vol. O2)		
Mass-flow rate	[kg/s]	0.049947
Temperature	[°C]	450

The coupled boundary condition means that both, convective and radiative heat flux is calculated on the cell face. Flue gas properties were defined by mixing laws except for the absorption coefficient, the thermal conductivity, and the viscosity. The absorption coefficient was calculated according to different model approaches (see section 3.3) and was implemented via an “User Defined Function” (UDF). The thermal conductivity and the viscosity of the flue gas were also implemented via an UDF as a function of the local mixture and temperature according to the NASA polynomial expressions [81]. A pressure outlet was defined at the top of the furnace’s chimney.

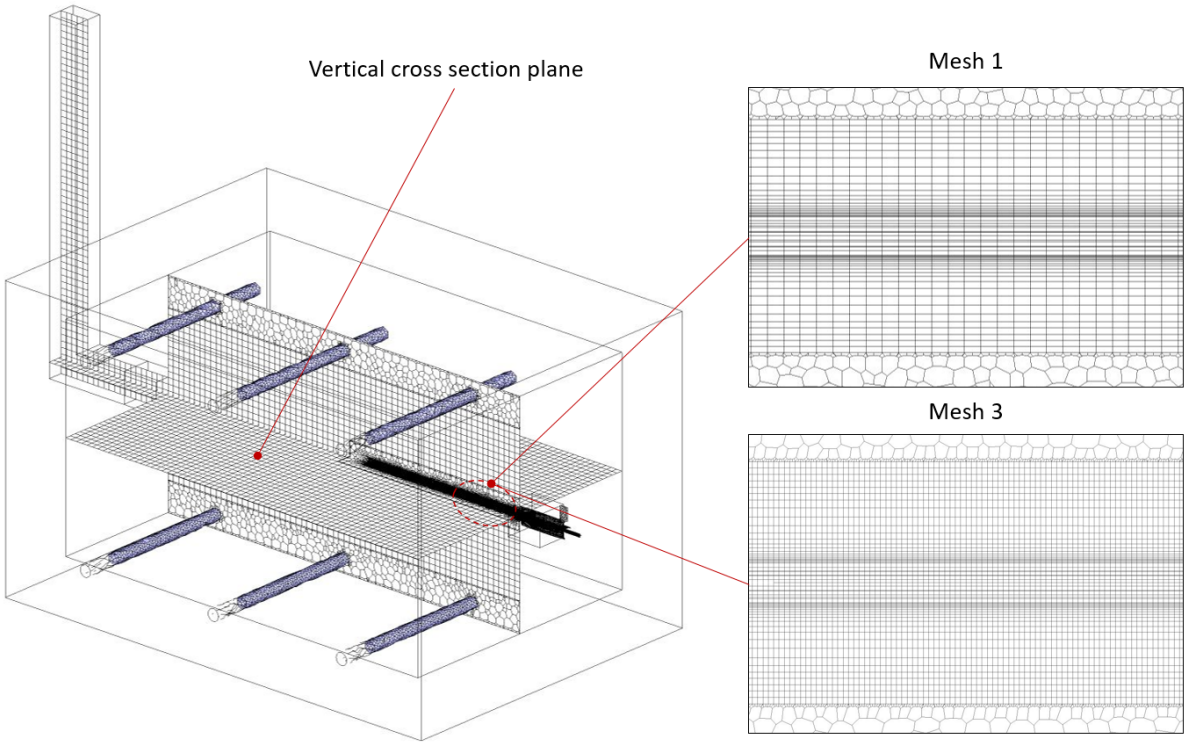

Figure 2. Global mesh of the burner test rig with details of reaction zone

4. Results

This section is subdivided into four parts: the model validation (section 4.1) where the accuracy of the presented methodology is evaluated with experimental data, an evaluation of different WSGG models (section 4.2) and an evaluation of different reaction mechanisms and combustion models (section 4.3). Furthermore, a comparison of flameless combustion of natural gas and hydrogen is performed in section 4.4. This includes an analysis of the reaction zone and the heat transfer behaviour and a thermal efficiency evaluation.

4.1. Grid independency and model validation

The furnace model in this work is based on the grid independency study of a previous work with similar configuration but with natural gas as fuel [59]. Nevertheless, further evaluation of the grid independency was performed based on “Mesh 1” in [59] with two refinement levels (Mesh 2 and Mesh 3). For this investigation, the PP-SFM model and the “GRI 3.0”

were applied for the simulations. The predicted temperatures in the furnace thermocouples (Figure 4 left) and in the burner's axis (Figure 4 right) of each mesh were used for the evaluation. The results show that "Mesh 1" and "Mesh 2" predicted quite similar results in each thermocouple (Figure 4 left) and deviations were only observed in the burner's axis. Thus, a further refinement ("Mesh 3") was only done with the cells in the reaction zone through which the total number of cells didn't double. The results of "Mesh 2" and "Mesh 3" showed quite similar results in the thermocouples and in the burner's axis (Figure 4 right) with only a slight deviation at the position of 305 mm in the burner's axis. Thus, further refinement of "Mesh 3" is not necessary and grid independency is ensured. Furthermore, it was found that a finer grid resolution in the reaction zone is necessary in comparison to flameless combustion of natural gas (see "Mesh 1" in [59]). Nevertheless, "Mesh 3" was used for all further simulations in this study due to a slightly higher element quality. For a validation, the measured temperatures in the furnace thermocouples and in the burner's axis were also included in Figure 4 and compared with the predicted values of the CFD model. It becomes visible that the numerical results are in close accordance with the experimental data and maximal deviations by 15 K in the furnace thermocouples are obtained. Temperatures in the burner's axis have maximum deviations by 100 K to the experimental data at the measurement position at 1180 mm. In the section from 305 to 730 mm, the temperatures were underpredicted by the numerical model. The value and position of the maximum temperature was predicted in close accordance with the experimental data. In the region between 730 mm and 1405 mm, the model overpredicts the temperature in the burner axis. Overall, the results of this section show that flameless combustion of hydrogen needs a finer mesh in comparison to natural gas due to the higher gradients.

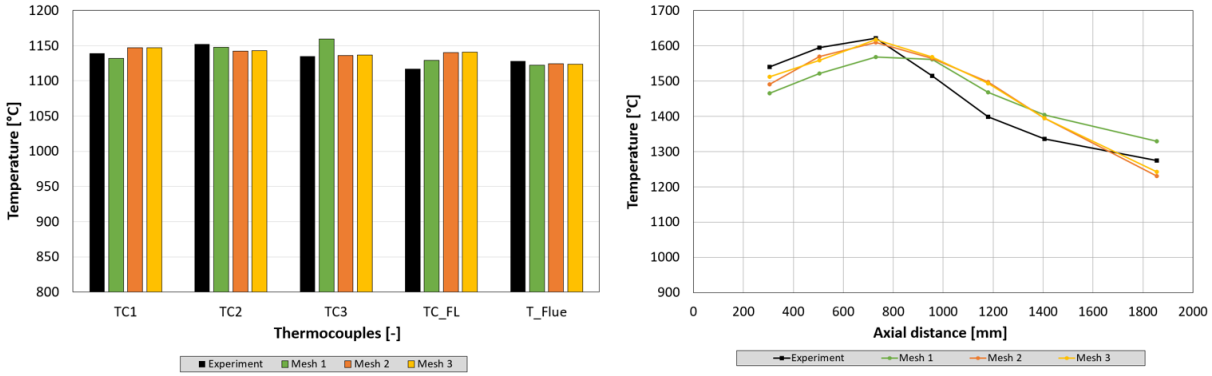

Figure 3. Measured and predicted temperatures in the thermocouples (left) and the burner's axis (right)

4.2. Comparison of different WSGG models

The accurate prediction of the radiative heat transfer is an important part, in combustion modelling. Therefore, the calculation of the absorption coefficient of the hot flue gases plays an important role and is mainly done by the WSGG model with the coefficients from Smith et al. [49]. In case of hydrogen combustion with air, the validity of this approach was evaluated and other sets of WSGGM coefficients were tested. The PP-SFM model and the "GRI 3.0" [28] reaction mechanism was used in all cases of the evaluation because it predicted the best results for a similar configuration with natural gas [59]. Figure 5 shows temperature values in each discrete measurement point in the burner axis of the different WSGGM approaches. A sphere volume with a diameter of 30 mm was used for the volume averaging of the temperature values. The results show that the models by Smith et al. [49] and Yin et al. [52], which are basically developed for the combustion of hydrocarbons, predicted quite similar temperatures along the burner axis. In general, each WSGG model predicted the highest temperature in the measurement points at the correct position of 730 mm. Between 305 and 530 mm away from the burner tip, the highest temperatures were obtained by the model coefficients from Yin et al. [52], which are in best accordance with the measurements. The coefficients from Bordbar et al. [54], which were developed for pure steam as flue gas, were also tested for their application in pure hydrogen flameless combustion. Results of this modelling approach show lower temperatures at 305 mm away from the

burner's nozzle. Starting from 955 mm to 1855 mm, the temperature distribution of this model coefficient predicted the best result in accordance with the experimental data. The models by Yin et al. [52] and Smith et al. [49] predicted quite similar, but higher temperatures in this region (> 900 mm) than the model by Bordbar et al. [54].

Radial temperature distributions at the axial positions 730 mm (full lines) and 1180 mm (dashed lines) from the experiments and the CFD simulations are also presented in Figure 5. The furnace temperature of 1150°C was reached at a radial distance of about 250 mm with all applied WSGG models. Yin et al. [52] and Smith et al. [49] predicted a similar radial temperature profile at the 730 mm position but with higher deviations from experimental data than the model by Bordbar et al. [54]. The best accordance with the measured temperature profile at the position of 1180 mm was also reached with the model by Bordbar et al. [54]. An evaluation of the non-gray gas approach with the models by Bordbar et al. [54] and Yin et al. [52] is presented in Figure 6. The more comprehensive non-gray gas approach predicted higher temperatures in the axial region between 305 and 730 mm (Figure 6 left), which is in better accordance with the experiment. Also, the highest measured temperature is in alignment with the result of the simulation. Only in the region between 1180 and 1800 mm, the non-gray approach predicted higher temperatures than the gray gas approach. The radial temperature distribution (Figure 6 right) looks similar to the results under gray gas assumption. Furthermore, the computational time for the non-gray gas model increases. Table 4 gives an overview of the maximum and averaged temperatures and absorption coefficients of each WSGG model. The coefficients from Smith et al. [49] and Yin et al. [52] determined lower averaged and maximum values for the absorption coefficients and the gas temperature in the combustion chamber than the model by Bordbar et al. [54] with gray gas assumption. Higher values for the absorption coefficient and the gas temperature were predicted by the non-gray approach.

Table 4: Parameters for the radiative heat transfer

WSGGM	DO Model	T_{gas_ave}	T_{gas_max}	k_{ave}	k_{max}
[-]	[-]	[°C]	[°C]	[1/m]	[1/m]
Smith et al.	gray	1139	1625	0.241	0.256
Yin et al.	gray	1138	1617	0.264	0.288
Bordbar et al.	gray	1142	1648	0.274	0.312
Yin et al.	non-gray	1152	1651	-	-
Bordbar et al.	non-gray	1157	1657	-	-

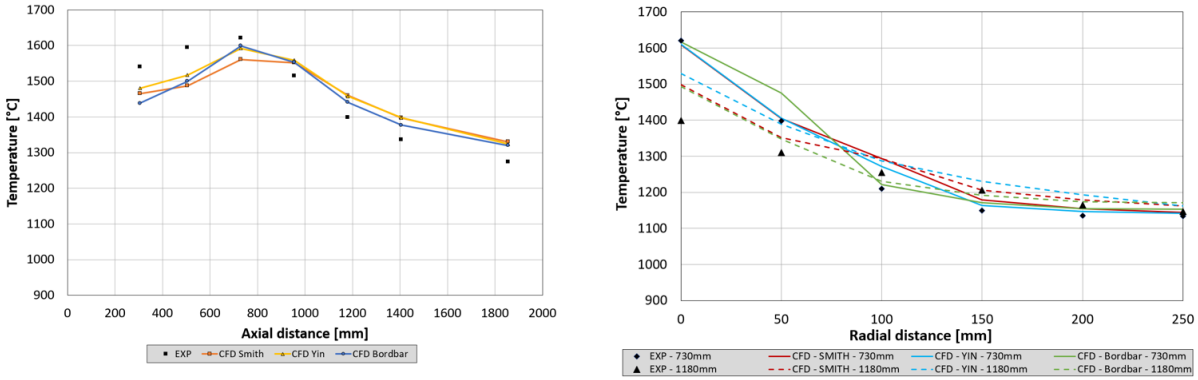

Figure 5. Axial and radial temperature distributions with gray WSGG models

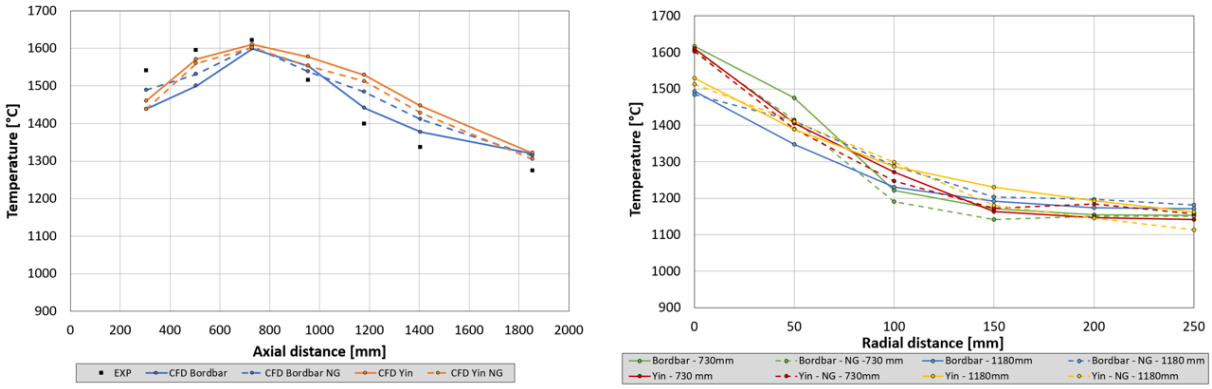

Figure 6. Axial and radial temperature distributions with non-gray WSGG models

Contour plots of the temperature and the absorption coefficient in a horizontal plane through the burner axis are presented in Figure 7. It becomes clear that the results for the temperature are quite similar in the burner axis according to the presented results in Figure 5. A comparison of the temperature region away from the central burner axis in the burner test rig shows similar results between the models by Smith et al. [49] and Bordbar et al. [54]. Only the WSGG model with the coefficients from Yin

et al. [52] predicted quite different results with a different shape of the temperature contour lines. Detailed plots of the temperature contours in the reaction zone are presented above the complete section planes. Different explorations and locations of the regions with the highest temperatures can be observed. In addition, contour plots of the absorption coefficient, which is the quantity directly predicted by the different model approaches, are also presented in Figure 7. The plots obtained by Smith et al. [49] and Yin et al. [52] are quite similar. The main deviation from the model by Bordbar et al. [54] cannot be detected in the reaction zone but in regions, where the combustion is completed. Based on the obtained results, the model coefficients from Bordbar et al. [54] and gray gas assumption were identified as well suited for the case in this paper.

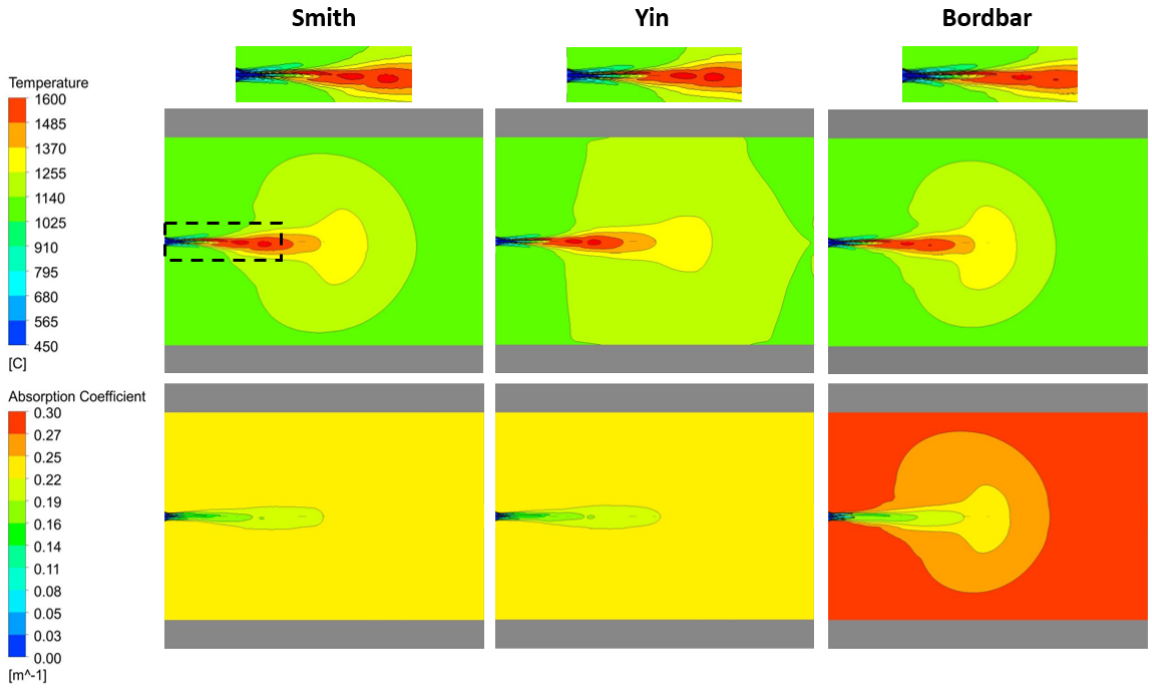

Figure 7. Temperature distribution in the burner axis with different WSGG models with gray gas assumption

4.3. Comparison of different combustion models and reaction mechanisms

An important issue in combustion modelling is the selection of the combustion model and the reaction mechanism for the present case. A

goal of this paper is the evaluation of different flamelet-based combustion models, which have the opportunity to use detailed reaction mechanisms without high computational time. Figure 8 shows the predicted temperatures of the three combustion models, namely the NP-SFM, the PP-SFM and the PP-FGM model as described in section 3.2. The “GRI 3.0” mechanism [28] and the gray WSGG model by Bordbar et al. [54] were used for the combustion model evaluation. The results show that the PP-SFM and NP-SFM models predicted a very similar temperature distribution over the whole burner axis (Figure 8 left). Slightly lower temperatures more in line with the experimental data were obtained by the NP-SFM in the intervals 955 - 1855 mm. It is visible that NP-SFM and PP-SFM underpredicted the temperatures from the burner’s nozzle up to 730 mm by observing the volume averaged values in the measurement points. In the section between 955 and 1855 mm, higher temperatures were predicted by these models with a maximum deviation by about 50 K from the experimental data. Satisfying results in accordance with the experimental data were obtained by the PP-FGM with diffusion type flamelets. Unfortunately, the PP-FGM fails at predicting the complete flameless combustion because an unburnt hydrogen content of 1.7 vol.% was obtained at the outlet. Thus, the energy balance and the predicted temperatures in the furnace thermocouples weren’t in close accordance with measured data at the outlet. The radial temperature distributions of all combustion models (Figure 8 right) showed close accordance with the experimental data at an axial position of 730 mm for all combustion models. Higher deviations up to 70 K are only present between the burners’ axis and 100 mm at the axial position of 1180 mm. In the next step, three detailed reaction mechanisms were evaluated for their performance in modelling flameless combustion of hydrogen with air. In this evaluation, the PP-SFM model and the WSSG model proposed by Bordbar et al. [54] were applied for the comparisons in this section. The results are presented in Figure 8. Quite similar temperature distributions were predicted by the mechanisms GRI 3.0 [28] and the mechanism by O’Conaire [73] in the burner’s axis (Figure 9 left). Slightly higher values were obtained by the second one in the region between 305 and 730 mm

which are more in line with the measurements. The Sandiego mechanism [72] fails at predicting the location and the value of the maximum temperature. An evaluation of the radial temperature profiles (Figure 9 right) shows similar temperature distributions at both observed axial positions but with higher deviations to the experimental data at 1180 mm.

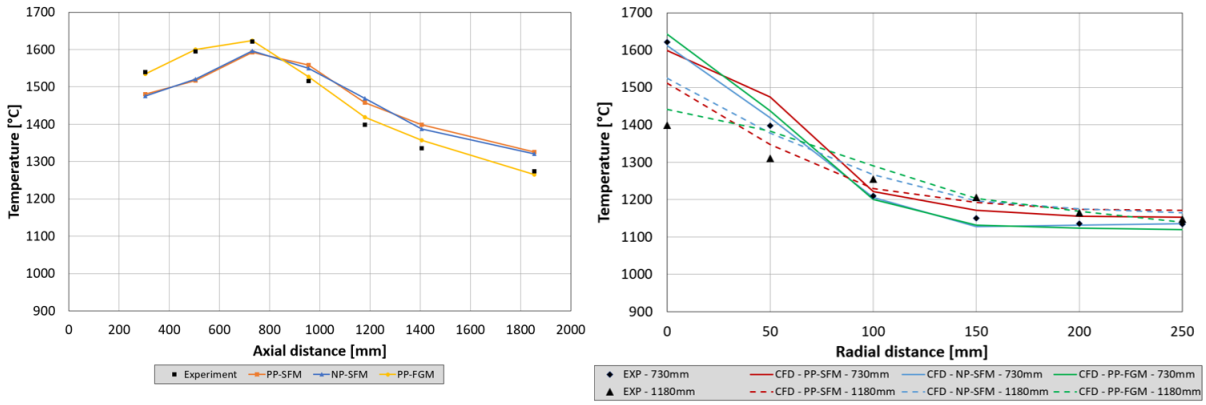

Figure 8. Temperature distributions with different combustion models

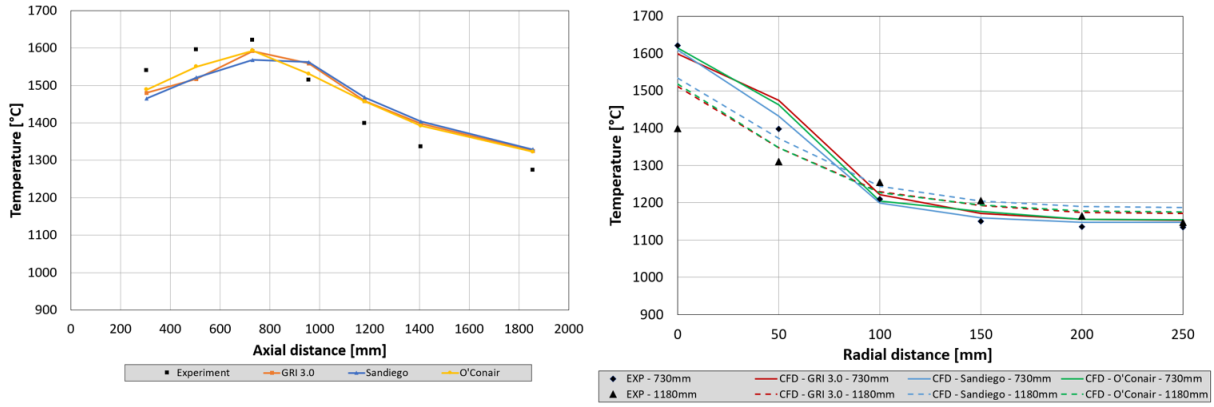

Figure 9. Temperature distributions with different reaction mechanisms

A concluding analysis of the temperature contour plots predicted by all evaluated models and mechanisms are presented in Figure 10. The observed plane is a horizontal cross-section through the burner's axis (see Figure 3). It is shown that the temperature regions further away from the reaction zone look quite similar for all applied mechanisms. Thus, the detailed contour plot of the reaction zone (marked with dashed lines) is presented above each global one, which show deviations from each other. The higher temperatures in the region from 305 to 955 mm obtained by the mechanism by O'Conaire [73] (Figure 9 left) depicted in the detailed contour plot show close accordance with the experimental

data. An interruption of the high temperature contour at a position of 505 mm predicted by the “GRI 3.0” and the “Sandiego” mechanism is also depicted in the detailed plots. This circumstance agrees with the axial temperature distribution in Figure 9. In case of the combustion model evaluation, a similar, global temperature distribution in the burner test rig was obtained by the PP-SFM and the NP-SFM. Only the PP-FGM model predicted a differently shaped contour in the range between 1286°C and 1391°C (yellow). A detailed view of the reaction zone contour plot below the global plots presents clearer deviations between the PP-FGM, NP-SFM and PP-SFM. Based on the obtained results, the NP-SFM with the mechanism by O’Conaire [73] was chosen for further calculations.

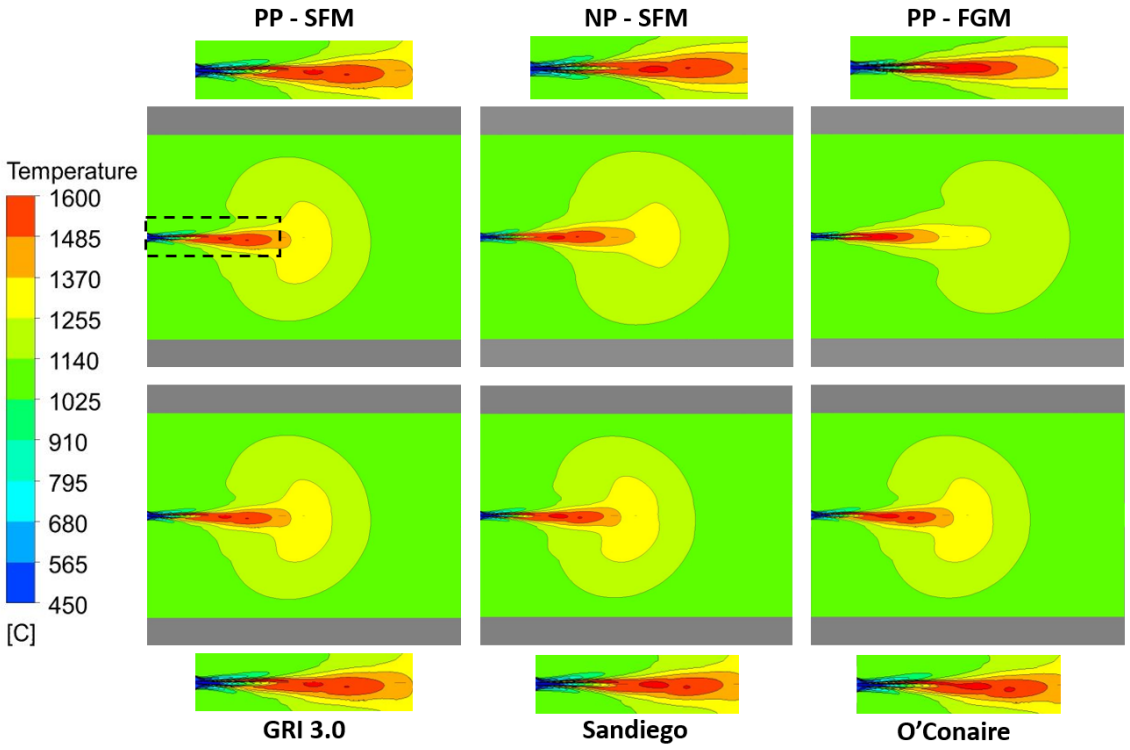

Figure 10. Temperature distribution in the burner axis with different combustion models and reaction mechanisms

4.4. Comparison between flameless combustion of natural gas and hydrogen

The model evaluations in the previous sections (4.1, 4.2, 4.3) show that a combination of the NP-SFM model and the mechanism by O’Conaire

[73] predicts the best results in accordance with the experimental data and the full burnout of hydrogen. The calculation of the absorption coefficient was done with the WSGG model coefficients from Bordbar et al. [54] for pure steam and with gray gas assumption in this case. Experimental data from the temperature field measurement and the corresponding results of the CFD model at a furnace temperature of 1150°C are presented in Figure 11. The orange line (Figure 11 left) represents the predicted volume-averaged temperature values at the measurement positions and the corresponding experimental data is illustrated with a black line. It is shown that the model approach predicts the temperatures in a close accordance with the experimental data from 305 mm to 1180 mm. At greater distances from the burner's nozzle, the model predicts higher temperatures as measured with maximum deviations of 50 K. A comparison with the well applied flameless combustion of natural gas is also included (Figure 11 left). The data of the natural case at an equal furnace temperature of 1150°C was taken from a previous study [59]. This dataset also includes measured and predicted temperatures from a validated CFD model. In case of natural gas application, the PP-SFM with the "GRI 3.0" mechanism predicted the most accurate results among the flamelet-based combustion models. The flameless combustion of hydrogen has a higher temperature level over the whole burner's axis. A difference between the maximum measured temperatures in each case of about 150 K was obtained at position of 955 mm away from the nozzle.

Figure 11 (right) presents the measured and volume averaged radial temperatures of flameless hydrogen combustion. It can be observed that maximum deviations between predicted and measured temperatures are present between 0 and 150 mm away from the burner axis. At measurement points which have a higher radial distance as 150 mm to the burner's axis, close accordance with the experimental data is achieved with the presented methodology. Figure 12 presents a comparison between the radial temperature profiles of pure hydrogen (full lines) and natural gas (dashed lines) as fuel for flameless combustion at different axial positions. Only experimental data is used in this

illustration. It is visible that the radial temperature profiles at hydrogen operation reach similar values as natural gas at a radial distance of about 200 mm. The radial temperature distributions are an important information for an evaluation of the burners position and the thermal load on the insulation.

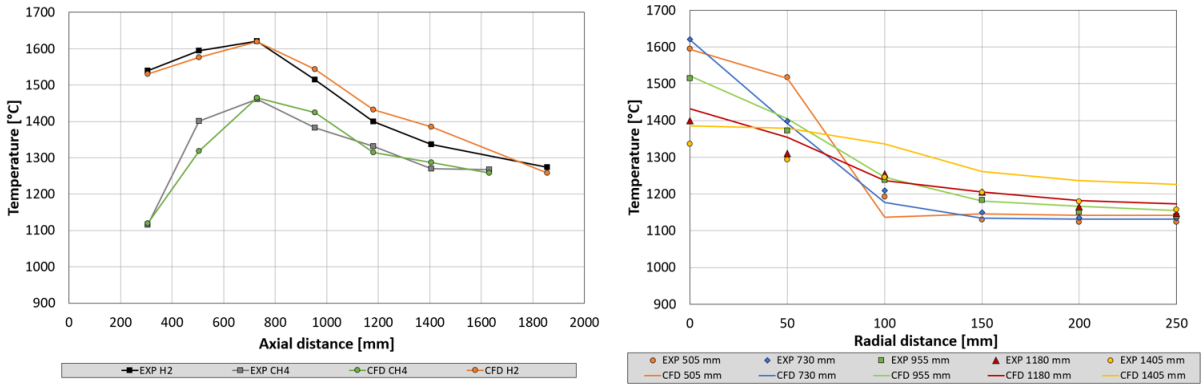

Figure 11. Axial (left) and radial (right) temperature distributions

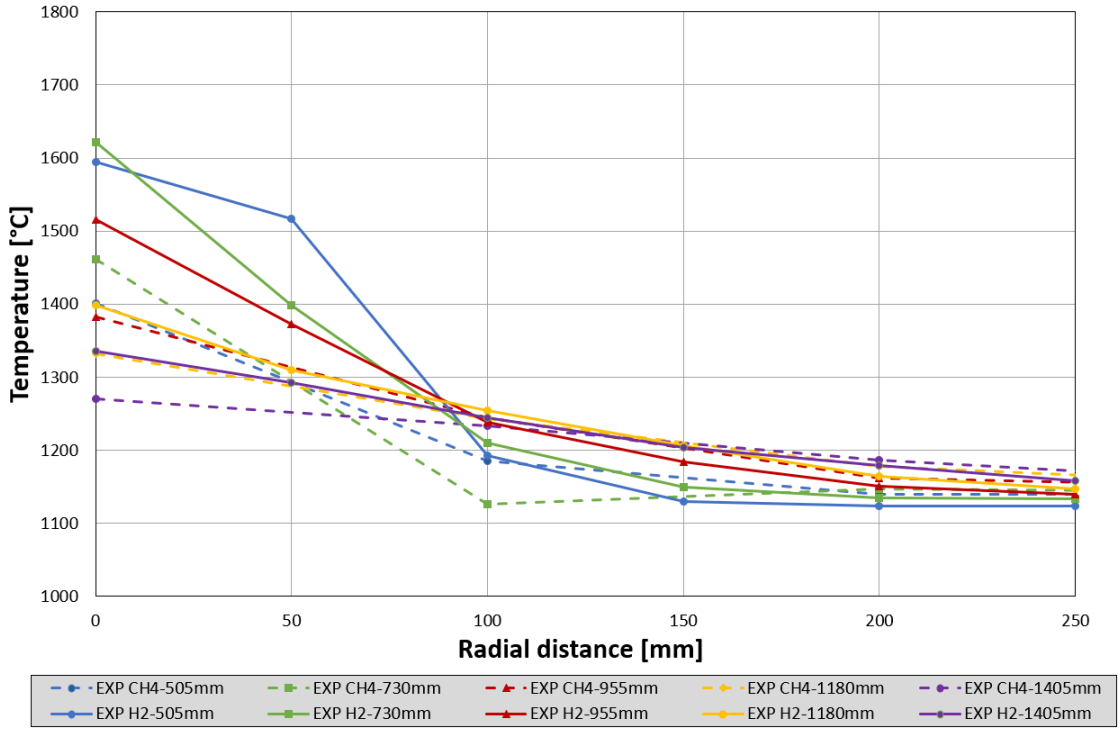

Figure 12. Radial temperature distributions of hydrogen and natural gas

Furthermore, the contour plots of the temperature, the velocity and the OH-radical species concentration for natural gas and hydrogen combustion are presented in Figure 13. By comparing the temperature plot it becomes clear that the temperature region above 1255 °C is more

extended and has different propagation at pure hydrogen operation. Higher reaction zone temperatures of about 1610°C are generally present with the application of hydrogen as fuel at similar furnace boundary conditions. By comparing the velocity contour plots it can be noticed that hydrogen operation has higher fuel nozzle velocities caused by the higher volume-flow rate in comparison to the natural gas case. Furthermore, the velocity region with values higher than 5 m/s is more extended in case of pure natural gas operation compared to hydrogen operation. This circumstance leads to a lower local mechanical load of the fibre insulation close to the burner position. Therefore, a fuel change of an existing heat treatment furnace to hydrogen can be made from the point of the maximum allowed fluid velocity. The contour plots of the OH-Radical volume fraction showed a higher concentration in the centre of the reaction zone at flameless hydrogen combustion compared to the natural gas case. Furthermore, the volumetric evolution of the OH concentration is slightly smaller at hydrogen operation.

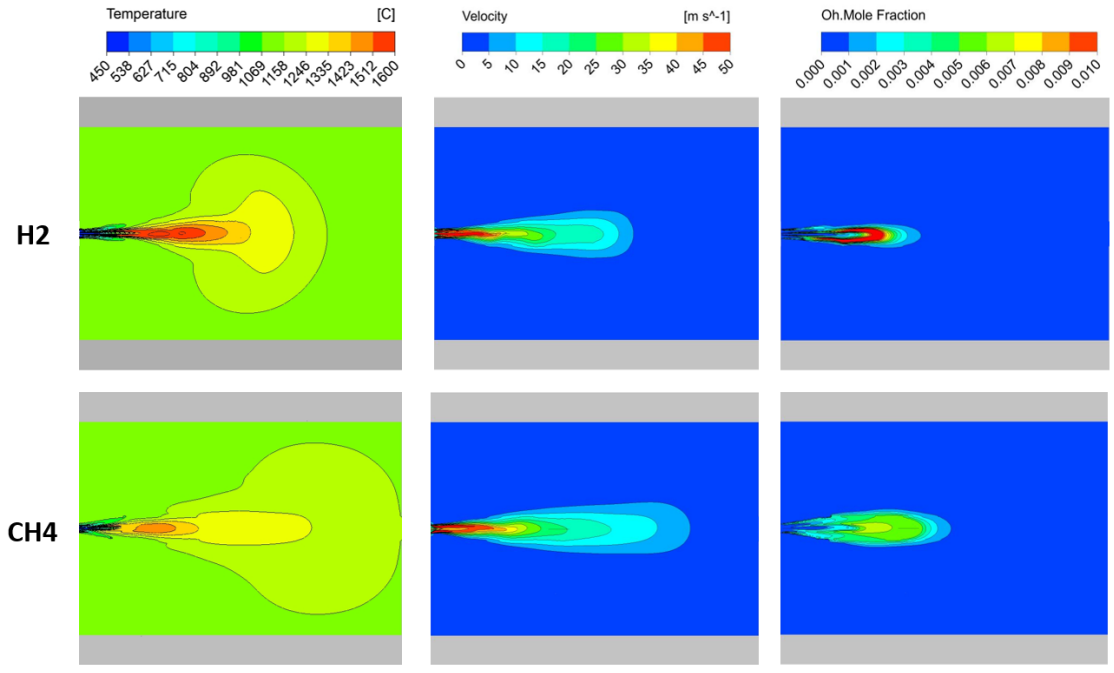

Figure 13. Temperature, velocity and OH concentration contour plot at H2 and CH4 operation

A study of Mayrhofer et al. [12] showed an efficiency increase by adding hydrogen to natural gas with a maximum content of 40 vol.%. Thus, the potential of a fuel change from pure natural gas to pure hydrogen is also

investigated in this section by CFD simulations. The flameless burner was operated with a nominal thermal input of 155 kW and an air to gas ratio that 3 vol.% oxygen in the flue gas is ensured. The results of the energy balance were compared with the data of a previously investigated case at flameless natural gas combustion [59]. Table 5 shows a heat flux comparison between hydrogen and natural gas operation. Deviations between the thermal input of the preheated combustion air are due to different stochiometric amounts of air for the different fuels. A furnace temperature of 1150°C in both cases leads to similar wall losses. It can be apparent that the flue gas loss is reduced by about 16 percent at hydrogen operation. Furthermore, an increased heat flux to the cooling tubes of about 24 percent from 34.3 up to 42.6 kW is observed in the simulations. A concluding evaluation of the combustion efficiency according to Eq. 9 was done for both experimental and numerical cases. The changed heat fluxes at hydrogen operation lead to an efficiency increase by about 7 percent.

$$\eta_{FP} = 1 - \frac{\dot{Q}_{Flue}}{\dot{Q}_{Fuel} + \dot{Q}_{Air\ preheat}} = 1 - \frac{\dot{m}_{flue\ gas}\ c_p|_0^{T_{flue\ gas}}\ T_{flue\ gas}}{\dot{m}_{fuel}\ LHV + \dot{m}_{air}\ c_p|_0^{T_{air}}\ T_{air}} \quad (9)$$

Table 5: Energy balance and efficiency from CFD models

Case [-]	$\dot{Q}_{Combustion}$ [kW]	$\dot{Q}_{Air}$ [kW]	$\dot{Q}_{Flue}$ [kW]	$\dot{Q}_{Tubes}$ [kW]	$\dot{Q}_{Wall}$ [kW]	η_{FP} [%]
CFD - H2	155	23.5	76.3	43.1	59.1	57
EXP - H2	155	23.5	78.3	43.1	57.1	56
CFD - CH4 [59]	155	29.2	93.4	30.9	60	49
EXP - CH4 [59]	155	29.2	92.4	30.9	61	50

5. Conclusion

The present work shows a 3D CFD modelling study of flameless combustion with pure hydrogen as fuel and highly-preheated air (450°C)

as an oxidizer. In order to keep the computational effort low, the main goal of the work was the development of an efficient modelling approach. This concerns the evaluation of different flamelet-based combustion models. Furthermore, experimental data from temperature field measurements of the reaction zone were used to present the suitability of the predicted temperature field in close accordance.

- A model of the burner test rig was developed and validated with experimental data. Maximum temperature deviation of 5 K at the furnace control thermocouples and about 50 K in the burner axis were observed.

- Three detailed reaction mechanisms, suggested by the literature and three flamelet-based combustion models were applied. The results show that the NP-SFM model with the mechanism proposed by O'Conaire et al. [73] predicts the best results in accordance with the experimental data and correct prediction of the heat losses.

- Gray and non-gray WSGG modelling approaches of the flue gas were evaluated caused by the changed composition. The coefficients for pure steam, suggested by Bordbar et al. [54] and gray gas assumption predicts the best results in accordance with the experimental data. The models by Yin et al. [52] and Smith et al. [49] predict higher deviations.

- A comparison of flameless combustion of natural gas and pure hydrogen shows differences in temperature field. Furthermore, efficiency increases by about 7 % was observed by the fuel change.

Acknowledgments

This work was supported by the Ebner Industrieofenbau GmbH and the Institute of Thermal Engineering, Graz University of Technology.

References

[1] J. A. Wünning and J. G. Wünning, Flameless oxidation to reduce thermal NO-formation, Progress in Energy and Combustion Science 23 (1997) pp. 81-94

[2] A. Cavalliere and M. Joannon, Mild Combustion, Progress in Energy and Combustion Science 30 (2004) pp. 329-366

[3] B. B. Dally, E. Riesmeier and N. Peters, Effect of fuel mixture on moderate and intense low oxygen dilution combustion, Combustion and Flame 137 (2004) pp. 418-431

[4] Federal Ministry for Environment, Nature Conservation and Nuclear Safety, Technical Instructions on Air Quality Control – TA Luft, 2002, Germany, https://www.bmu.de/fileadmin/Daten_BMU/Download_PDF/Luft/taluft_engl.pdf

[5] The European Parliament, Medium Combustion Plant Directive, 2015.

[6] United Nations, Kyoto Protocol, 1997, https://unfccc.int/resource/docs/convkp/kpeng.pdf.

[7] United Nations, Paris Agreement, 2015, https://unfccc.int/sites/default/files/english_paris_agreement.pdf.

[8] The European Comission, EU ETS Handbook, 2015, https://ec.europa.eu/clima/sites/clima/files/docs/ets_handbook_en.pdf.

[9] S. Bukhold, Blauer Wasserstoff - Perspektiven und Grenzen eines neuen Technologiepfades, Greenpeace Energy, Hamburg, 2020.

[10] J. D. Holladay, An overview of hydrogen production technologies, Catalysis Today 139 (2009) pp. 244-260

[11] M. A. Salam, K. Ahmed, N. Akter, T. Hossain and B. Abdullah, A review of hydrogen production via biomass gasification and its prospect in Bangladesh, International Journal of Hydrogen Energy 43 (2018) pp. 14944-14973

[12] M. Mayrhofer, M. Koller, P. Seemann, R. Prieler and C. Hochenauer, Assesment of natural gas / hydrogen blends as fuel for industrial heat treatment furncaces, International Journal of Hydrogen Energy 46 (2021) pp. 21672-21686

[13] R. Weber, S. Orsino, N. Lallemant and A. Verlaan, Combustion of natural gas with high-temperature air, Proceedings of the Combustion Institute 28 (2000) pp. 1315–1321

[14] M. Derudi and R. Rota, Experimental study of the mild combustion, Proceedings of the Combustion Institute 33 (2011) pp. 3325–3332

[15] R. Weber, On the combustion of gaseous, liquid and solid fuels in high temperature preheated air, Proceedings ot the combustion institute 30 (2005) pp. 2623-2629

[16] H. Zhou, T. A. Ring and J. C. Sutherland, Additional criteria for MILD coal combustion, Proceedings of the Combustion Institute (2020), https://doi.org/10.1016/j.proci.2020.06.175

[17] M. Saha, B. B. Dally, P. R. Medwell and A. Chinnici, Effect of particle size on the MILD combustion characteristics of pulverised, Fuel Processing Technology 155 (2017) pp. 74-87

[18] M. Derudi, A. Villani and R. Rota, Mild Combustion of Industrial Hydrogen-Containing Byproducts, Industrial & Engineering Chemistry Research 46 (2007) pp. 6806-6811

[19] M. Skottene and K. Rian, A study of NOx formation in hydrogen flames, International Journal of Hydrogen Energy 32 (2007) pp. 3572-3585

[20] M. Ayoub, C. Rottier, S. Carpentier, C. Villermaux, A. M. Boukhalfa and D. Honore´, An experimental study of mild flameless combustion, International Journal of Hydrogen Energy 37 (2012) pp. 6912-6921

[21] L. D. Arteaga Mendez, M. J. Tummers, E. H. van Veen and D. J. E. M. Roekaerts, Effect of hydrogen addition on the structure of natural-gas jet-in-hot-coflow flames, Proceedings of the Combustion Institute 35 (2015) pp. 3557–3564

[22] G. J. RØRTVEIT, K. ZEPTER, Ø. SKREIBERG, M. FOSSUM and J. E. HUSTAD, A comparison of Low-NOx burners for combustion of methane, Proceedings of the Combustion Institute 29 (2002) pp. 1123–1129

[23] F. Donatini, M. Schiavetti, G. Gigliucci, P. Gheri, M. Monticelli, R. Mangione, R. Paulozza and J. Riccardi, CFD simulation and experimental tests on a natural gas/hydrogen mixture-fired flameless combustor, ENEL-GEM-Area Tecnica Ricerca, Pisa, Italy.

[24] C. Galletti, A. Parente, M. Derudi, R. Rota and L. Tognotti, Numerical and experimental analysis of NO emissions from a lab-scale burner fed with hydrogen-enriched fuels and operating in MILD combustion, International Journal of Hydrogen Energy 34 (2009) pp. 8339–8351

[25] A. Parente, C. Galletti and L. Tognotti, Effect of the combustion model and kinetic mechanism on the MILD combustion in an industrial burner fed with hydrogen enriched fuels, International Journal of Hydrogen Energy 33 (2008) pp. 7553–7564

[26] S. Ivarone, M. Cafiero, M. Ferrarotti, F. Contino and A. Parente, A multiscale combustion model formulation for NOx predictions in hydrogen enriched jet flames, International Journal of Hydrogen Energy 44 (2019) pp. 23436-23457

[27] R. Bilger, S. Starner and R. Kee, On reduced mechanisms for methane-air combustion in non-premixed flames, Combustion and Flame 80 (2) (1990) pp. 135-149

[28] G. P. Smith, D. M. Golden, M. Frenklach, N. W. Moriarty, B. Eiteneer, M. C. Goldenberg, T. Bowman, R. K. Hanson, S. Song, J. W. C. Gardiner and V. V. Lissianski, GRI-MECH 3.0, http://combustion.berkeley.edu/gri_mech/

[29] A. Kazakov and M. Frenklach, Reduced reaction sets based on GRI 1.2 Mech, http://combustion.berkeley.edu/drm/.

[30] M. S. Cellek and A. Pinarbasi, Investigations on performance and emission characteristics of an industrial low swirl burner while burning natural gas, methane, hydrogen-enriched natural gas and hydrogen as fuels, International Journal of Hydrogen Energy 43 (2018) pp. 1194-1207

[31] M. S. Cellek, Flameless combustion investigation of CH4/H2 in the laboratory-scaled furnace, International Journal of Hydrogen Energy 45 (2020) pp. 35208-35222

[32] A. Mardani and H. K. M. Mahalegi, Hydrogen enrichment of methane and syngas for MILD combustion, International Journal of Hydrogen Energy 44 (2019) pp. 9423-9437

[33] A. Mardani, Optimization of the Eddy Dissipation Concept (EDC) model for turbulence-chemistry interactions under hot diluted combustion of CH4/H2, Fuel 191 (2017) pp. 114-129

[34] A. De, E. Oldenhof, P. Sathiah and D. Roekaerts, Numerical Simulation of Delft-Jet-in-Hot-Coflow (DJHC) Flames Using the Eddy Dissipation Concept Model for Turbulence–Chemistry Interaction, Flow, Turbulence and Combustion 81 (2011), pp. 537–567

[35] A. Parente, M. R. Malik, F. Contino, A. Cuoci and B. B. Dally, Extension of the Eddy Dissipation Concept for turbulence/chemistry, Fuel 163 (2016) pp. 98-111

[36] J. Aminian, C. Galletti and L. Tognotti, Extended EDC local extinction model accounting finite-rate chemistry, Fuel 165 2016 pp. 123-133

[37] P. Li, F. Wang, J. Mi, B. B. Dally, Z. Mei, J. Zhang and A. Parente, Mechanism of NO formation in MILD combustion of CH4/H2 fuel blends, International Journal of Hydrogen Energy 39 (33) (2014) pp. 19187-19203

[38] Y. B. Zeldovich, Oxidation of Nitrogen in Combustion and Explosions, European Physical Journal A. Hadrons and Nuclei 21 (1946) pp. 577-628

[39] C. P. Fenimore, Formation of nitric oxide in premixed hydrocarbon flames, Proc Combust Inst 13 (1971) pp. 373–379

[40] A. A. Konnov, G. Colson and J. de Ruyk, The New Route Forming NO Via NNH, Combustion and Flame 121 (2000) pp. 548-550

[41] P. C. Malte and D. T. Pratt, Measurement of atomic oxygen and nitrogen oxides in jet-stirred combustion. Symposium (International) on combustion 15 (1) (1975) pp. 1061-1070

[42] C. Galletti, M. Ferrarotti, A. Parente and L. Tognotti, Reduced NO formation models for CFD simulations of MILD combustion, International Journal of Hydrogen Energy 40 (2015), pp. 4884-4897

[43] G. Ali, T. Zhang, W. Wu and Y. Zhou, Effect of hydrogen addition on NOx formation mechanism and pathways in MILD combustion of H2-rich low calorific fuels, International Journal of Hydrogen Energy 45 (2020), pp. 9200-9210

[44] V. Fortunato, G. Mosca, D. Lupant and A. Parente, Validation of a reduced NO formation mechanism on a flameless furnace fed with H2-enriched low calorific value fuels, Applied Thermal Engineering 144 (2018) pp. 877-889

[45] A. Parente, C. Galletti and L. Tognotti, A simplified approach for predicting NO formation in MILD combustion of CH4-H2 mixtures, Procedings to the Combustion Institute 33 (2) (2011) pp. 3343-3350

[46] N. Kim, Y. Kim, M. N. M. Jaafar, M. . R. Rahim and M. Said, Effects of hydrogen addition on structure and NO formation of highly CO-Rich syngas counterflow nonpremixed flames under MILD combustion regime, International Journal of Hydrogen Energy 46 (2021) pp. 10518-10534

[47] G. D. Raithby and E. H. Chui, A finite-volume method for predicting a radiant heat transfer in enclosures with participating media, Journal of Heat Transfer 112 (1990) pp. 415-423

[48] E. H. Chui and G. D. Raithby, Computation of radiant heat transfer on a non-orthogonal mesh using the finite-volume method, Numerical Heat Transfer Part B: Fundamentals 23 (1993) pp. 269-288

[49] T. F. Smith, Z. F. Shen and J. N. Friedman, Evaluation of coefficients for the weighted sum of grey gases model, Journal of Heat Transfer 104 (1982) pp. 602-608

[50] G. Krishnamoorthy and M. Jimenez, Non-gray modeling of radiative heat transfer in hydrogen combustion scenarios, International Journal of Energy Research 36 (2012), pp. 789-797

[51] D. W. Green and M. Z. Southard, Perry's Chemical Engineer's Handbook, MacGraw-Hill Education, 2019, New York, ISBN: 978-0-07-183409-4

[52] C. Yin, L. C. R. Johansen, L. A. Rosendahl and S. K. Kaer, New Weighted Sum of Gray Gases Model Applicable to Computational Fluid Dynamics (CFD) Modelling of Oxy-Fuel Combustion: Derivation, Validation, and Implemention, Energy Fuels 24 (2010) pp. 6275-6282

[53] M. H. Bordbar, G. Wecel and T. Hyppänen, A line by line based weighted sum of gray gases model for inhomogeneous CO2-H2O mixture in oxy-fired combustion, Comubstion and Flame 161 (2014) pp. 2435-2445

[54] H. Bordbar, G. C. Fraga and S. Hostikka, An extended weighted-sum-of-gray-gases model to account for all CO2 - H2O molar fraction ratios in thermal radiation, International Communications in Heat and Mass Transfer 110 (2020) pp. 104400

[55] A. Chitgarha and A. Mardani, Assessment of steady and unsteady flamelet models for MILD combustion modeling, International Journal of Hydrogen Energy 43 (2018) pp. 15551-15563

[56] A. Mardani and S. Tabejamaat, Effect of hydrogen on hydrogenemethane turbulent non-premixed flame under MILD condition, International Journal of Hydrogen Energy 35 (2010) pp. 11324-11331

[57] M. Ferrarotti, W. De Paepe and A. Parente, Reactive structures and NOx emissions of methane/hydrogen mixtures in flameless combustion, International Journal of Hydrogen Energy 46 (2021) pp. 34018-34045

[58] Y. Afarin and S. Tabejamaat, Effect of hydrogen on H2/CH4 flame structure of MILD combustion using the LES method, International Journal of Hydrogen Energy 38 (2013) pp. 3447-3458

[59] M. Mayrhofer, M. Koller, P. Seemann, R. Prieler and C. Hochenauer, Evaluation of flamelet-based combustion models for the use in a flameless burner under different operating conditions, Applied Thermal Engineering 183 (2021) pp. 116190

[60] S. V. Patanker, Numerical heat transfer and fluid flow, Taylor & Francis, 1980, e-ISBN:9781315275130

[61] ANSYS Inc., ANSYS Fluent Therory Guide 13.0, Cannonsbourg, 2015

[62] T. H. Shih, W. W. Liou, A. Shabbir, Z. Yang and J. Zhur, A new k-ε eddy viscosity model for high Reynolds number turbulent flows, Computational Fluids 24 (1995) pp. 227-238

[63] R. Prieler, B. Mayr, M. Demuth, D. Spoljaric and C. Hochenauer, Application of the steady flamelet model on a lab-scale and an industrial furnace for different oxygen concentrations, Energy 91 (2015) pp. 451-464

[64] B. Mayr, R. Prieler, M. Demuth, C. Potesser and C. Hochenauer, Computational analysis of a semi-industrial furnace fired by a flat flame burner under different O2/N2 ratios using the steady laminar flamelet approach, Journal of the energy institute 90 (4) (2017) pp. 602-612

[65] D. Tabacco, C. Innarella and C. Bruno, Theoretical and numerical investigation on flameless combustion, Combustion Science and Technology 174 (7) (2002), pp. 1-35

[66] B. F. Magnussen and B. H. Hjertager, On mathematical modeling of turbulent combustion with special emphasis on soot formation and combustion, in 16th Symposium (Int) on combustion (1977), The combustion institute

[67] B. F. Magnussen, On the structure of turbulence and a generalized eddy dissipation concept for chemical reaction in turbulent flow, in: 19th AIAA meeting, St. Louis, USA, 1981

[68] M. Mayrhofer, M. Koller, P. Seemann, H. Bordbar, R. Prieler and C. Hochenauer, M. Mayrhofer, M. Koller, P. Seemann, R. Prieler, C. Hochenauer, CFD investigation ofa vertical annealing furnace for stainless steel and non-ferrous alloys strips – A comparative study on air-staged& MILD combustion, Thermal Science and Engineering Progress (2021), doi: https://doi.org/10.1016/j.tsep.2021.101056

[69] N. Peters, Laminar diffusion flamelet models in non-premixed turbulent combustion, Progress in Energy and Combustion Science 10 (1984) pp. 319-339

[70] N. Peters, Laminar flamelet concepts in turbulent combustion, 21st Symposium (Int) on combustion (1986), The combustion Institute

[71] J. van Ojien and L. P. de Goey, Modelling of premixed laminar flames using flamelet-generated manifolds, Combustion Science and Technology 161 (2000) pp. 113-137

[72] Chemical-Kinetic Mechanisms for Combustion Applications, San Diego Mechanism Web page, https://web.eng.ucsd.edu/mae/groups/combustion/mechanism.html.

[73] M. O Conaire, H. J. Curran, J. M. Simmie, W. J. Pitz and C. K. Westbrook, A Comprehensive Modeling Study of Hydrogen Oxidation, International Journal of Chemical Kinetics Volume 36 (11) (2004) pp. 603-622

[74] P. S. Cumber and M. Fairweather, Evaluation of flame emission models combined with the discrete transfer method for combustion system simulation, International Journal of Heat and Mass Transfer 48 (2005), pp. 5221–5239

[75] R. Johansson, B. Leckner, K. Andersson and F. Johnsson, Account for variations in the H2O to CO2 molar ratio when modelling gaseous radiative heat transfer with the weighted-sum-of-grey-gases model, Combustion and Flame 158 (2011) pp. 893-901

[76] L. J. Dorigon, G. Duciak, R. Brittes, F. Cassol, M. Galarca and F. H. R. Franca, WSGG correlations based on HITEMP2010 for computation of thermal radiation in non-isothermal, non-homogeneous H2O/CO2 mixtures, International Journal of Heat and Mass Transfer 64 (2013), pp. 863-873

[77] T. Kangwanpongpan, F. H. Franca, R. Correa da Silva, P. Smith Schneider and H. J. Krautz, New correlations for the weighted sum of gray gases model in oxy fuel conditions based on HITEMP 2010 database, International Journal of Heat and Mass Transfer 55 (2012) pp. 7419–7433

[78] C. Yin, Refined Weighted Sum of Gray Gases Model for Air-Fuel Combustion and Its Impacts, Energy & Fuels 27 (2013) pp. 6287-6294

[79] C. Yin, L. A. Rosendahl and S. K. Kaer, Chemistry and radiation in oxy-fuel combustion: A computational fluid dynamics study, Fuel 90 (2011) pp. 2519-2529

[80] C. Yin, Nongray-Gas Effects in Modeling of Large-Scale Oxy-Fuel Combustion Processes, Energy & Fuels 26 (2012) pp. 3349-3356

[81] B. J. McBridge, G. Sanford and M. A. Reno, Coefficients for calculating thermodynamic and transport properties of individual species, NASA, 1993, https://shepherd.caltech.edu/EDL/PublicResources/sdt/refs/NASA-TM-4513.pdf